Journal of Solid State Chemistry **152,** 286–301 (2000)
doi:10.1006/jssc.2000.8704, available online at http://www.idealibrary.com on IDEAL®

Simple Quaternary Ammonium Ions R_4N^+ (R = *n*Pr, *n*Bu, *n*Pen) as Versatile Structure Directors for the Synthesis of Zeolite-Like, Heterobimetallic Cyanide Frameworks

Eyck-Michael Poll, Sabine Samba, R. Dieter Fischer,[1] Falk Olbrich,* Nicola A. Davies,† Paolo Avalle,† David C. Apperley,† and Robin K. Harris†

*Institut für Anorganische und Angewandte Chemie der Universität Hamburg, Martin-Luther-King-Platz 6, 20146 Hamburg, Germany; *Chemisches Institut, Otto-von-Guericke-Universität Magdeburg, Universitätsplatz 2, 39106 Magdeburg, Germany; and † Department of Chemistry, University of Durham, South Road, Durham DH1 3LE, UK*

The preparation of three new examples of water insoluble host/guest assemblies of the general composition: [(R_4N)($Me_3Sn)_2M(CN)_6 \cdot zH_2O$] ($R$ = *n*-propyl or *n*-pentyl, M = Fe or Co, $0 \leq z \leq 2$) from likewise polymeric *super*-Prussian-blue derivatives [$(Me_3Sn)_3M(CN)_6$] and aqueous (R_4N)X solutions are reported. According to combined single-crystal X-ray (3a and 3a*: R = *n*Pr, M = Co, z = 2; 5b: R = *n*Pen, M = Fe, z = 0.5), powder X-ray diffraction (XRD), and multinuclear (^{13}C, ^{15}N, ^{59}Co, ^{119}Sn) CPMAS solid-state magnetic resonance studies, 3a and 3a* contain *cis*- and *trans*-isomeric $[Co(CN)_4(CNSnMe_3OH_2)_2]^-$ building blocks, respectively, which are held together exclusively by Sn ← OH_2 ··· NC–Co hydrogen bonds. In striking contrast, the building blocks of 5b and 5a are infinite [M–CN–Sn–NC] chains. In all these assemblies, also significant C–H ··· NC hydrogen bonds between the encapsulated R_4N^+ guest ion and exclusively terminal cyanide ligands of the host seem to play a notable auxiliary role. © 2000 Academic Press

Key Words: **metal cyanides; heterometallic, polymeric; organotin(IV) fragments; quaternary ammonium ions; solid state NMR (^{13}C, ^{15}N, ^{59}Co, ^{119}Sn).**

INTRODUCTION

Quaternary ammonium ions are essential for the synthesis of many zeolites in playing the role of structure-directing "templates" (1), although calcined zeolites deprived of the initially encapsulated ammonium ions are usually of major interest. Polymeric metal cyanides may likewise adopt numerous two- or three-dimensional (2D or 3D) framework structures (2), and *hetero*(bi)metallic polymeric cyanide may even share several characteristic properties with zeolites. A rapidly increasing number of cyanide-based host/guest systems containing inter alia tetraalkylammonium guest ions (3–10) has been obtained, in close analogy to "as-synthesized" zeolites, in aqueous media from salt-like and molecular precursors, respectively, of the final constituents of the anticipated host/guest systems. In contrast to most zeolites, however, these products are chemically too unstable to survive an appropriate calcination procedure.

On the other hand, several initially R_4N-free cyanide-based frameworks may readily be transformed, just by suspension in aqueous solutions of R_4N^+-salts, into still polymeric R_4N-containing derivatives, although one particular component of the initial framework is extruded (9). Correspondingly facile "remodeling" reactions of *zeolites* leading "back" to as-synthesized R_4N-containing products are practically unknown, although zeolite dealumination (1,11) represents likewise the facile attack of an alumosilicate skeleton. Another way of enriching in R_4N^+ ions is through the formal uptake of (R_4N)OH by a polymer from aqueous solution. In contrast to the simple exchange of a H^+ or H_3O^+ guest ion by a R_4N^+ competitor, some initially R_4N-free metal cyanides may in fact incorporate an OH^- ion into the host framework, and concomitantly the R_4N^+ ion into a likewise available cavity (8).

In the present contribution, two new examples of "exchange"-based remodeling reactions involving the attack of R_4N^+ ions on polymeric *super*-Prussian-blue systems [$(Me_3Sn)_3M(CN)_6$] (12) will be described and compared with the results of corresponding coprecipitation experiments. Particular attention will be focused here on the surprisingly different structure-directing properties of the closely related tetraalkylammonium ions R_4N^+ with R = methyl (Me), ethyl (Et), *n*-propyl (*n*Pr), *n*-butyl (*n*Bu) (9), *n*-pentyl (*n*Pen), and *n*-hexyl (*n*Hex). In considering here each of these tetraalkylammonium ions as an individually reacting synthon, "supramolecular interactions" based on "noncovalent" bonds (i.e., coordinative bonds, hydrogen bonds, Van der Waals forces, etc.) between the host and the guest constituents of the zeolite-related polymeric

[1] To whom correspondence should be addressed. Fax: (+49) 40-42838-2882. E-mail: fischer@chemie.uni-hamburg.de.

0022-4596/00 $35.00

metal cyanides are seen to become increasingly more important.

EXPERIMENTAL

Materials

Designation of the starting systems of type **2** = $[(Me_3E)_3M(CN)_6]$. **2a** $E = Sn$, $M = Co$; **2b**: $E = Sn$, $M = Fe$; **2c**: $E = Pb$, $M = Co$. $[(nPr_4N)(Me_3E)_2M(CN)_6 \cdot 2H_2O]$ (**3a** and **3a***: $E = Sn$, $M = Co$; **3b**: $E = Sn$, $M = Fe$; **3c**: $E = Pb$, $M = Co$). Product **3a** was prepared from **2a** (12) and nPr_4NI as described in Ref. 9 (sample "2*e*"). ν(CN) bands (cm^{-1}, IR): 2137, 2144; Raman: 2150, 2157, 2173. Anal. Calcd. For $C_{24}H_{50}N_7O_2CoSn_2$ (765.06): C 37.68, H 6.69, N 12.82. Found: C 37.48, H 6.58, N 12.69%. ^{15}N-enriched **3a** (CN ligands only, ca. 98%): IR 2105, 2113. Yield: 78%. The white product decomposes at 300°C in adopting a blue color. **3b**: A 500-mg (0.711 mmol) measure of **2b** (12) was suspended in a solution of 180.0 mg (0.811 mmol) of nPr_4NCl in 30 mL of H_2O. After stirring (12 h), filtration, washing (ca. 20 mL of H_2O), and drying, 450 mg (yield: 90.0%) of a lemon-yellow, light-sensitive product was obtained. ν(CN) bands (cm^{-1}, IR): 2125, 2136. Anal. Calcd. for $C_{24}H_{50}N_7O_2FeSn_2$ (761.97): C 37.83, H 6.61, N 12.87, O 4.20. Found: C 36.80, H 6.43, N 12.73, O 4.17. **3a***: A solution of $K_3[Co(CN)_6]$ (217 mg, 0.653 mmol) in H_2O (ca. 10 mL) was added under stirring to a solution of nPr_4NCl (144 mg, 0.650 mmol) and Me_3SnCl (260 mg, 0.652 mmol) in H_2O (ca. 20 mL). After a reaction period of ca. 15 min, the mixture was filtered and the residue washed with a small portion of H_2O. The white product was dried at room temperature (ca. 10 h) to afford air stable, analytically pure **3a***. Yield: 450 mg (90%). Exemplaric for the majority of products: ^1H NMR (200 MHz, D_2O/NaOD, pH ca. 9): $\delta = 0.59$ (s, 18 H, Me_3Sn), 0.94 (t, 12 H, γ-Me), 1.70 (m, 8 H, β-CH_2), 3.16 (m, 8 H, α-CH_2). IR (cm^{-1}) for ν-CN: 2137, 2147, 2158, 2174; Ra (cm^{-1}) for ν-CN: 2149, 2160, 2175. Above 300°C, the color changes from white to blue. Anal. Calcd. For $C_{24}H_{50}N_7O_2CoSn_2$ (765.06): C 37.68, H 6.59, N 12.82, O 4.18. Found: C 37.45, H 6.67, N 12.73, O 4.23%. **3c**: preparation as for **3b** from 500 mg (0.514 mmol) of **2c** (13) and 114.1 mg (0.514 mmol) of nPr_4NCl in 30 mL of H_2O. Yield: 90 mg (18%). At 230°C the white substance affords a blue, solid foam which turns black at ca. 350°C. ν(CN) band (cm^{-1}, IR): 2128. Anal. Calcd. for $C_{24}H_{50}N_7O_2CoPb_2$ (942.04): C 30.60, H 5.35, N 10.41, O 3.40. Found: C 30.50, H 5.33, N 10.34, O 3.45%. $[(nPen_4N)(Me_3Sn)_2M(CN)_6 \cdot 0.5H_2O]$ (**5a**, **5a***: $M = Co$; **5b**, **5b***: $M = Fe$). The preparation of **5a** from 300 mg (0.425 mmol) of **2a** and 160.72 (0.425 mmol) of $nPen_4NBr$ (in 30 mL of H_2O) follows that of **3a** and **3b**. Yield: 260 mg (86.6%). ν(CN) bands (cm^{-1}, IR): 2144; (Raman): 2159, 2176. Anal. Calcd. for $C_{32}H_{64}N_7O_{0.5}CoSn_2$ (850.21): C 45.21, H 7.47, N 11.53, O 0.94. Found: C 44.88, H 7.32, N 11.59, O 0.70%. **5a***: A solution of $K_3[Co(CN)_6]$ (116.0 mg, 0.349 mmol) in H_2O (ca. 10 mL) is added under stirring to a solution of Me_3SnCl (139.1 mg, 0.698 mmol) and $nPen_4NBr$ (132.1 mg, 0.349 mmol) in H_2O (ca. 10 mL). After filtration, washing, and drying, the white precipitate turns out to be pure **5a***. Yield: 100 mg (86.2%). ν(CN) bands (cm^{-1}, IR): 2144; (Raman): 2155, 2174. Decomp. temp. (partially liquid): 135–140°C; formation of solid foam: 200°C; blue color: ca. 295°C. Anal. Calcd. for $C_{32}H_{64}N_7O_{0.5}CoSn_2$ (850.21): C 45.21, H 7.47, N 11.53. Found: C 43.02, H 7.14, N 11.22. **5b**: Preparation as for **5a** from **2b** (300 mg, 0.426 mmol) and $nPen_4NBr$ (242.1 mg, 0.639 mmol) dissolved in 30 mL of H_2O. Yield: 250 mg (83.3%); color: lemon-yellow. ν(CN) band (cm^{-1}, IR): 2130. Decomp. (blue color): 172–180°C; black product: 300°C. Anal. Calcd. for $C_{32}H_{64}N_7O_{0.5}FeSn_2$ (847.13): C 45.37, H 7.50, N 11.57, O 0.94. Found: C 45.22, H 7.18, N 11.44, O 0.36%. **5b***: Preparation as for **5a*** from $K_3[Fe(CN)_6]$ (330 mg, 1.002 mmol), Me_3SnCl (279.3 mg, 1.402 mmol), and $nPen_4NBr$ (265.2 mg, 0.701 mmol). Yield: 300 mg (90.9%), color: lemon-yellow. ν(CN) band (cm^{-1}, IR): 2131. Decomp.: As for **5b**. Anal. Calcd. for $C_{32}H_{64}N_7O_{0.5}FeSn_2$ (847.13): C 45.37, H 7.50, N 11.57. Found: C 45.08, H 7.29, N 11.61%. Metal analyses (i.e., of $E = Sn$ or Pb and $M = Fe$ or Co) had to be omitted as the diverse other instrumental techniques adopted (vide supra) did not leave the samples in sufficient quantities.

Methods

Correct R_4N/Me_3E ratios of all samples containing the diamagnetic $[Co(CN)_6]^{3-}$ ion were deduced independently by inspection of the ^1H NMR spectra of solutions in D_2O/NaOD (pH $\sim$ 12). NMR spectrometers used: either Varian Gemini 200 BB (see above for **3a***) or Bruker AM 360. Infrared spectra were obtained on a Perkin-Elmer IR-1720 spectrometer and Raman spectra on a Jobin Yvon U-1000 instrument.

Single crystals suitable for X-ray crystallography were recovered from the filtrates obtained during the syntheses of **3a**, **3a***, and **5b** (vide supra). Crystal structure determinations were performed using a Syntex P2$_1$ four-circle diffractometer (for **3a**) and an axs Smart-CCD diffractometer (for **3a*** and **5b**), respectively (see also Table 2). While no absorption correction was carried out for **3a**, absorption corrections based on symmetry equivalent reflections using the SADABS program were accounted for instantaneously by the Smart-CCD diffractometer. The structures were solved by direct methods and refined by a full-matrix least-square procedure against F_2 with SHELXS-97 and SHELXL-97. Crystallographic data for **3a**, **3a***, and **5b** have been deposited with the Cambridge Crystallographic Data Centre. (Copies may be obtained free of charge on application to the Director, CCDC, 12 Union Road, Cambridge CB2 1EC, UK. Fax: int. code + 44(0) 1223/336-033. E-mail: deposit @chemcrys.cam.ac.uk.)

X-ray powder diffractograms were obtained on a Philips PW 1050 instrument (Cu$K\alpha$ source and Ni filter). Powder diagrams were simulated with CERIUS^2 3.0 (MSI), for the 2Θ range 5°–70°. The simulated XRD of **3a*** was subsequently improved by means of the Diffraction-Crystal software of CERIUS^2, assuming here a preferred orientation of crystallites in fitting the March–Dollase function (13) with the following parameters: $a = 0.00$, $b = 0.05$, $c = 0.00$, and R_o 0.65. The solid state NMR spectra were recorded on a Varian Unity Plus 300 spectrometer operating at frequencies of 75.43, 11.85, 30.40, and 71.13 MHz for ^{13}C, ^{119}Sn, ^{15}N, and ^{59}Co, respectively. Cross-polarization with high-power proton decoupling was implemented for all spectra except ^{59}Co, where direct polarization was used. The ^{13}C and ^{15}N spectra were recorded with a Doty Scientific probe containing 7-mm-o.d. rotors, but for the ^{119}Sn and ^{59}Co spectra a faster-spinning Doty Scientific probe with 5-mm-o.d. rotors was usually used. Acquisition conditions are given in the figure captions. Chemical shifts are reported, with the high-frequency positive convention, in ppm relative to the signals for $SiMe_4$, $SnMe_4$, NH_4NO_3 (nitrate line), and $K_3[Co(CN)_6]$(aq.) for ^{13}C, ^{119}Sn, ^{15}N, and ^{59}Co, respectively.

PREPARATION OF POLYMERIC R_4N-CONTAINING METAL CYANIDES INVOLVING $\{M(CN)_6\}$ BUILDING BLOCKS

The layered coordination polymer $[(Me_3Sn)_4Fe(CN)_6]$ **1** which contains per formula unit two *trans*-oriented, terminal $CNSnMe_3$ groups (14, 15) is known to exchange exactly one Me_3Sn^+ unit by, e.g., one Et_4N^+ ion (16), but only half a Me_3Sn^+ equivalent by the corresponding amount of $n$$Bu_4N^+$ ions (along with one H_2O molecule) (7):

$$[(Me_3Sn)_4Fe(CN)_6] + xR_4N^+ \xrightarrow{H_2O} [(R_4N)_x(Me_3Sn)_{4-x}Fe(CN)_6 \cdot yH_2O] + xMe_3Sn \cdot aq^+ \quad [1]$$

$$R = \text{Et}: x = 1.0,\ y = 0 \quad [1a]$$

$$R = n\text{Bu}: x = 0.5,\ y = 1. \quad [1b]$$

The driving force of both reactions is most probably the tendency of the two tetracoordinate tin atoms of **1** to adopt also pentacoordination. Actually, both of the sparingly soluble products and the dissolved $Me_3Sn \cdot aq^+$ ion (Eq. [1]) involve trigonal bipyramidal (tbp) Me_3Sn derivates, the two axial ligands being here NC and/or OH_2. On the other hand, the more recently reported (9) reaction according to Eq [2] is devoid of any change of the coordination number of the Sn atoms:

$$\underset{\text{(insoluble)}}{[(Me_3Sn)_3M(CN)_6]} + R_4N^+ \xrightarrow{H_2O} \underset{\text{(insoluble)}}{[(R_4N)(Me_3Sn)_2M(CN)_6 \cdot zH_2O]} + Me_3Sn \cdot aq^+ \quad [2]$$

2a: M = Co **3–5** (R = nPr, nBu (9), nPen; z = 0–2).

2b: M = Fe

At a first sight, two of the six coordinative N → Sn bonds present per formula unit of **2a**/**b** (12) are substituted by two coordinative O → Sn bonds (i.e., in $Me_3Sn \cdot aq^+$), although the O → Sn bond seems to be energetically less favorable than the CN → Sn bond. At least the facile, spontaneous precipitation of **2** (12) from solutions containing both $Me_3Sn \cdot aq^+$, and $[M(CN)_6]^{3-}$ ions (in the absence of $n$$Pr_4N^+$, $n$$Bu_4N^+$, and $n$$Pen_4N^+$ ions) strongly advocates for a superiority of the CN → Sn bond. Interestingly, in the presence of the larger R_4N^+ ions (i.e., R > Et), coprecipitation leads to the R_4N-containing products **3*–5*** (Eq. [3]), while even in the presence of any of the smaller ions Me_4N^+ and Et_4N^+ exclusively the *super*-Prussian-blue derivative **2** results (9):.

$$R_4N^+ + 2\,Me_3Sn \cdot aq^+ + [M(CN)_6]^{3-} \xrightarrow{H_2O} [(R_4N)(Me_3Sn)_2M(CN)_6 \cdot zH_2O]\downarrow \quad [3]$$

(R = nPr, z = 2, nBu, z = 1 (9), nPen; M = Co or Fe, z = 0.5).

In striking contrast to its closely related $n$$Pen_4N^+$ homolog, the $n$$Hex_4N^+$ ion neither attacks **2** (Eq. [2]) nor is it coprecipitated according to Eq. [3].

As all three Me_3Sn units of **2** are intrinsic constituents of its infinite 3D framework (12), reactions according to Eq. [2] are more appropriate examples of the "exchange type" than those according to Eq. [1]. In the latter case, which is not considered further, the leaving Me_3Sn^+ ion has just been anchored to the basic framework of **1** via *one* CN → Sn bond (15). The supramolecular architecture of the exchange product **4b** (R = nBu, M = Fe, z = 1) has recently been described (9). In the following sections, the crystal structures of the two new *exchange* products **3a** (R = nPr, M = Co, z = 2) and **5b** (R = nPen, M = Fe, z = 0.5) and of the coprecipitation product **3a*** will be presented and compared with the results of multinuclear high-resolution CPMAS solid-state magnetic resonance studies of **3a**/**3a***, **4a** (9), and **5a**. For more clarity, the numbering scheme of the

TABLE 1
Numbering Scheme of the R_4N-Containing Assemblies of the Type: $[(R_4N)(Me_3Sn)_2M(CN)_6 \cdot zH_2O]$

Number[a]	R	z	M = Co	M = Fe
3	*n*-Propyl	2	**a**	**b**
4	*n*-Butyl (9)	1	**a**	**b**
5	*n*-Pentyl	0.5	**a**	**b**

Note. For **1** and **2** see Eqs. [1] and [2], respectively.
[a] Symbol without a star, product prepared by Me_3Sn exchange (Eq. [2]); starred symbol (not included in the table) product obtained by coprecipitation (Eq. [3]).

assemblies to be discussed in more detail below is explained by Table 1.

RESULTS

Crystal Structures of 3a *and* 3a*

While structural identity of **4a** with its homologs **4a***, **4b**, and **4b*** has been successfully deduced from combined powder X-ray diffractometry (XRD), CPMAS NMR spectroscopy and the single-crystal X-ray study of **4b** (9), **3a**, and **3a*** turn out to have significantly different crystal structures and solid-state NMR spectra, although elemental analyses leave no doubt about the existence of two *isomeric* species. Selected crystal and refinement parameters of **3a** and **3a*** are included in Table 2, and relevant bond distances and angles of the two isomers are listed in Tables 3 and 4. The asymmetric units of the anionic components of **3a** and **3a*** are depicted in Fig. 1. In contrast to the initial assumption (vide supra), not two, but four of the potentially more favorable coordinative N → Sn bonds are replaced by O → Sn bonds during the formation of **3a** from **2a** (see Eq. [2]). The asymmetric units of **3a** and **3a*** contain, moreover, *one* nPr_4N^+ ion each, with four crystallographically nonequivalent *n*-propyl groups. In contrast to **3a***, the nPr_4N^+ ion of **3a** is disordered in that its central nitrogen atom (N4) adopts two slightly different positions (N4 ··· N4′ distance: 1.16(3) Å). Actually, **3a** contains the *cis*-isomer of the *trans*-configured $[Co(CN)_4(CNSnMe_3OH_2)_2]^-$ anion present in the lattice of **3a***. While in **3a*** only one of the two oxygen atoms is disordered, two different sets of tin-bonded methyl carbon atoms (designated as A and B) are found in the structure of **3a**. While the C(Me)–Sn–O and C(Me)–Sn–N angles of **3a*** scatter more closely around 90°, the methyl carbon atoms of set A are bent away from the oxygen atom (toward the nitrogen atom N1), whereas the carbon atoms of the other set (B) are bent toward the oxygen atom (Table 3). Somewhat surprisingly, this evidence of potential disorder is not accompanied by alternative positions of any of

TABLE 2
Crystallographic Parameters of 3a, 3a*, and 5b

	3a	**3a***	**5b**
Empirical formula	$C_{24}H_{50}N_7O_2CoSn_2$	$C_{24}H_{50}N_7O_2CoSn_2$	$C_{64}H_{120}N_{14}Fe_2Sn_4O$
Formula weight	765.02	765.02	1688.20
Crystal system	Orthorhombic	Orthorhombic	Monoclinic
a (Å)	11.478(3)	18.6990(2)	19.6796(2)
b (Å)	14.893(10)	18.6298(2)	15.56840(10)
c (Å)	10.706(4)	20.3276(2)	28.59780(10)
β (°)	90.00	90.00	103.83
V (Å^3)	1830.1(15)	081.30(13)	8507.85(11)
Z	2	8	4
Space group	$P2_12_12$	$Pbca$	$P2_1/n$
T (K)	293(2)	173(2)	173(2)
λ(Mo$K\alpha$) (Å)	0.71073	0.71073	0.71073
ρ_{calc} (g/cm^3)	1.381	1.435	1.318
μ (mm^{-1})	1.829	1.891	1.530
F (000)	764	3088	3448
θ Range of data collection (°)	2.34–32.56	1.84–28.36	1.14–29.23
Index ranges	$-2<h<17, -4<k<22, -2<I<16$	$-19<h<24, -24<k<24, -19<I<27$	$-26<h<25, -20<k<11, -39<I<37$
No. of reflcns collection	5567	47864	56835
No. of indep reflcns	4747 [R (int) = 0.0403]	8817 [R (int) = 0.0249]	21962 [R(int) = 0.0275]
No. of obsd reflcns [$I > 2\sigma(I)$]	3477	7759	16626
No. of data/estraints/parameters	4747/36/237	8817/0/408	21962/0/808
Goodnees-of-fit of F^2	1.037	1.101	1.036
R indices [$I > 2\sigma(I)$]	$R_1 = 0.0701$, $R_w^2 = 0.1732$	$R_1 = 0.0217$, $R_w^2 = 0.0441$	$R_1 = 0.0377$, $R_w^2 = 0.0783$
R indices (all data)	$R_1 = 0.0918$, $R_w^2 = 0.2013$	$R_1 = 0.0281$, $R_w^2 = 0.0465$	$R_1 = 0.0607$, $R_w^2 = 0.0895$
Largest diff. peak and hole (e Å^{-3})	0.483 and −1.459	0.605 and −0.726	1.562 and −1.578

Note. $w = 1/[s^2(F^2) + (xP)^2 + yP]$, where $P = (Fo^2 + 2Fc^2)/3$; **3a** ($x = 0.0972$, $y = 2.5604$); **3a*** ($x = 0.0143$, $y = 4.9788$); **5b** ($x = 0.00263$, $y = 14.7884$).

TABLE 3
Selected Interatomic Distances (Å) and Angles (°) of 3a (*i* = 4–6)

Sn–N1	2.324(11)	Sn–C4A	2.163(11)
Sn–O	2.289(8)	Sn–C5A	2.171(11)
		Sn–C6A	2.170(10)
Sn–N1–C1	160.5(12)	Sn–C4B	2.176(10)
N1–Sn–O	178.2(5)	Sn–C5B	2.168(10)
		Sn–C6B	2.153(10)
O ··· N2	2.694(16)	C7 ··· N3	3.13(3)
O ··· N3	2.674(15)	C10 ··· N2	3.17(4)
		C16 ··· N2	3.56(3)
N1–Sn–C4A	84.4(16)	O–Sn–C4A	95.7(16)
N1–Sn–C5A	85.2(19)	O–Sn–C5A	93.1(18)
N1–Sn–C6A	86.6(9)	O–Sn–C6A	95.0(9)
N1–Sn–C4B	101.9(14)	O–Sn–C4B	79.2(13)
N1–Sn–C5B	92.3(8)	O–Sn–C5B	85.9(8)
N1–Sn–C6B	94.8(9)	O–Sn–C6B	86.0(9)
$(N1–Sn–CiA)_{ave}$ 85.4; $(N1–Sn–CiB)_{ave}$ 96.3°		$(O–Sn–CiA)_{ave}$ 94.6	
		$(O–Sn–CiB)_{ave}$ 83.4	

Note: Dotted lines refer to O–H ··· N and C–H ··· N hydrogen bonds, respectively (only C ··· N distances < 3.70 Å have been considered).

the adjacent non-hydrogen atoms. Most of the interatomic distances and bond angles of **3a** and **3a*** are quite similar and compare likewise well with corresponding data reported for **4b** (9).

TABLE 4
Selected Interatomic Distances (Å) and Angles (°) of 3a*

Sn1–N1	2.289(2)	Sn1–C7	2.109(2)
Sn2–N2	2.329(2)	Sn1–C8	2.119(2)
Sn1–O1	2.28(1)	Sn1–C9	2.113(3)
Sn1–O3	2.27(2)	Sn2–C10	2.119(2)
Sn2–O2	2.257(2)	Sn2–C11	2.119(2)
		Sn2–C12	2.115(2)
Sn1–N1–C1	169.7(2)	N1–Sn1–C7	91.08(9)
Sn2–N2–C2	178.1(2)	N1–Sn1–C8	91.09(8)
N1–Sn1–O1	173.0(4)	N1–Sn1–C9	90.98(9)
N1–Sn1–O3	172.0(9)	N2–Sn2–C10	90.32(8)
N2–Sn2–O2	174.91(6)	N2–Sn2–C11	90.63(8)
		N2–Sn2–C12	92.58(9)
O1 ··· N4	2.74(2)	O1–H–N4	146(4)
O1 ··· N5	2.77(2)	O1–H–N5	165(3)
O3 ··· N4	2.72(3)	O3–H–N4	158(5)
O3 ··· N5	2.74(3)	O3–H–N5	155(4)
O2 ··· N3	2.713(2)	O2–H–N3	174(3)
O2 ··· N6	2.679(2)	O2–H–N6	171(3)
C22 ··· N4	3.366(3)[a]	C13 ··· N3	3.550(3)[a]
C19 ··· N5	3.454(3)[a]	C24 ··· N4	3.616(3)
C20 ··· N3	3.455(3)	C16 ··· N4	3.642(3)[a]
C21 ··· N3	3.512(3)	C23 ··· N6	3.680(3)
C23 ··· N4	3.527(3)		

Note. Dotted lines refer to O–H ··· N and C–H ··· N hydrogen bonds, respectively (only C ··· N distances < 3.70 Å have been considered)
[a] α-CH_2 group.

The supramolecular architectures of the two isomers **3a** and **3a*** have in common that, in striking contrast to the structures of, e.g., **2** (12) and **4b** (9), extended [M–CN–E–NC] chains are absent. Instead, adjacent *cis* (or *trans*-)-configured $[Co(CN)_4(CNSnMe_3OH_2)_2]^-$ ions are interconnected by significant O–H ··· NC hydrogen bonds to infinite, negatively charged 3D frameworks. Perspectives of the packing modes of the anions of **3a** and **3a*** are compared in Fig. 2. For each isomer, four distinct O–H ··· NC bonds are found per formula unit. Somewhat more instructive visualizations with respect to the hydrogen bonds and the positions of the encapsulated nPr$_4$N$^+$ ions of **3a** are given in Figs. 3 and 4.

As in the structure of **4b** (9), (α-)C ··· N distances short enough to suggest also significant C–H ··· NC hydrogen bonding between α-CH_2 groups of the R_4N^+ ion and (exclusively) terminal cyanide N atoms are found in the 3D frameworks of both **3a** and **3a*** (Tables 3 and 4). Interestingly, isomer **3a** with *cis*-configured $\{Co(CN)_4(CNSn)_2\}$ fragments displays both slightly shorter O–H ··· NC and C–H ··· NC hydrogen bonds than **3a***. The two C–H ··· N interactions C7 ··· N3 and C10 ··· N2, with 3.13(3) and 3.17(4) Å, respectively, belong to the shortest C–H ··· NC bonds so far known. For instance, Desiraju et al. have reported (17) C ··· N distances of 3.471(4) and 3.516(6) Å for the C–H ··· N≡C interactions in 2D "polymeric" 1,3,5-tricyanobenzene. The less conventional C–H ··· NC hydrogen bonds present in **3a** and **3a*** are probably also responsible for the almost nondisordered nature of their nPr$_4$N$^+$ guest ions.

Crystal Structure of 5b

Although, according to elemental analyses and XRD-studies, apparently isostructural products of the composition: $[(n\mathrm{Pen}_4\mathrm{N})(\mathrm{Me}_3\mathrm{Sn})_2\mathrm{M(CN)}_6 \cdot 0.5\mathrm{H}_2\mathrm{O}]$ with $M = \mathrm{Co}$ (**5a**) and Fe (**5b**) were obtained both by Me_3Sn exchange (Eq. [2]) and by coprecipitation (Eq. [3]), single crystals suitable for crystallographic X-ray studies could so far be obtained only for **5b**. In view of a more "appropriate insolubility" (i.e., for crystallization) in water, the nPen$_4$N-containing assemblies with $M = \mathrm{Fe}$ seem to resemble those containing the nBu$_4$N$^+$ ion (9). The asymmetric unit of **5b** (Fig. 5, which also presents the atomic numbering scheme) reveals that this supramolecular structure involves (i) infinite [*M*–CN–Sn–NC] chains, but (ii) no tin-coordinated water molecules, (iii) two crystallographically nonequivalent $\{Fe(CN)_6\}$ units (with two terminal CN ligands each) and nPen$_4$N$^+$ ions, respectively, and (iv) only two *n*-pentyl groups with disordered methyl ends. This type of structure differs totally from those of **3a** and **3a*** and in some respects also from that of **4b**. In contrast to **3a**/**a*** and **4b**, where each Co/Fe atom carries four and three terminal cyanide ligands, respectively, each Fe atom of **5b** involves no more than two

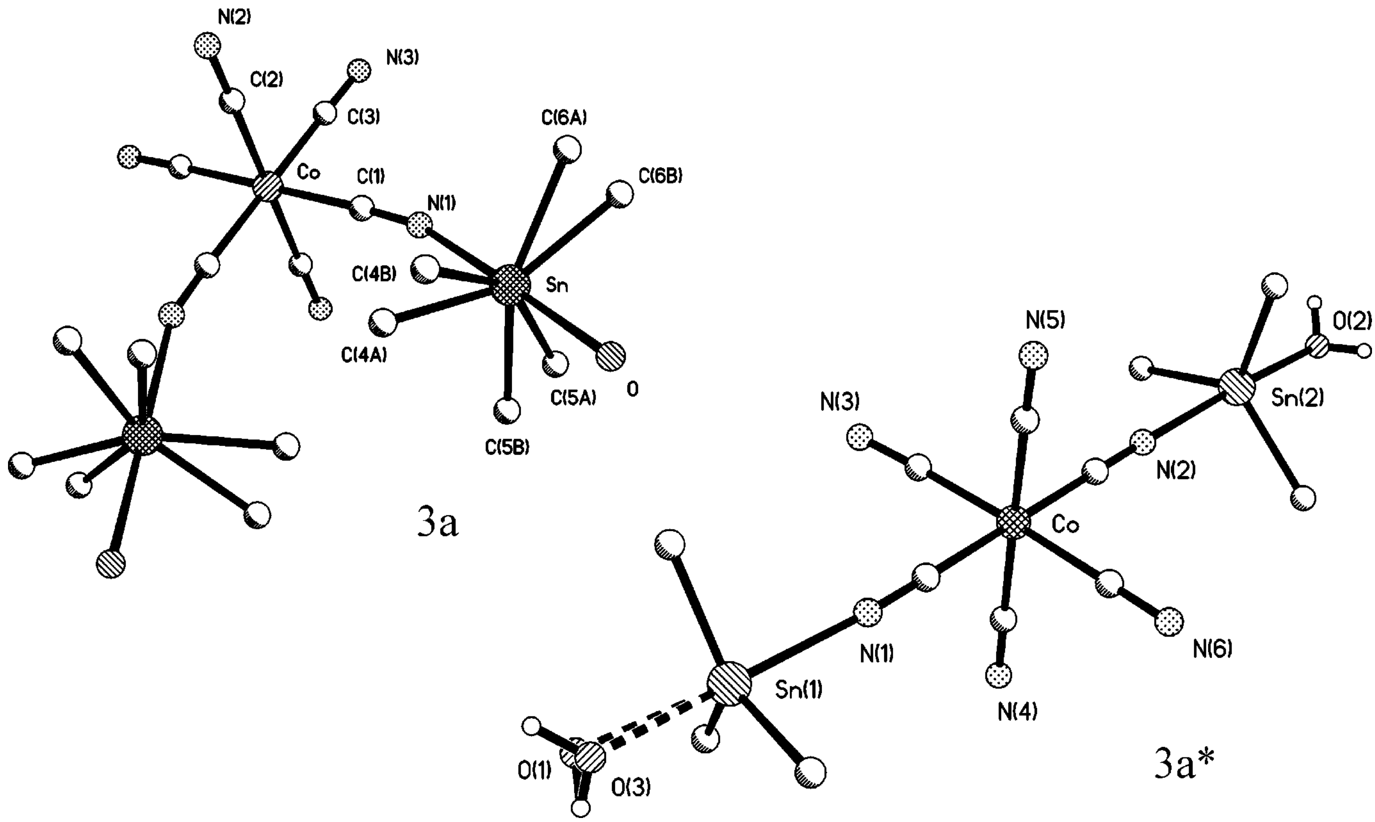

FIG. 1. Asymmetric units of the anionic components of **3a** and **3a***.

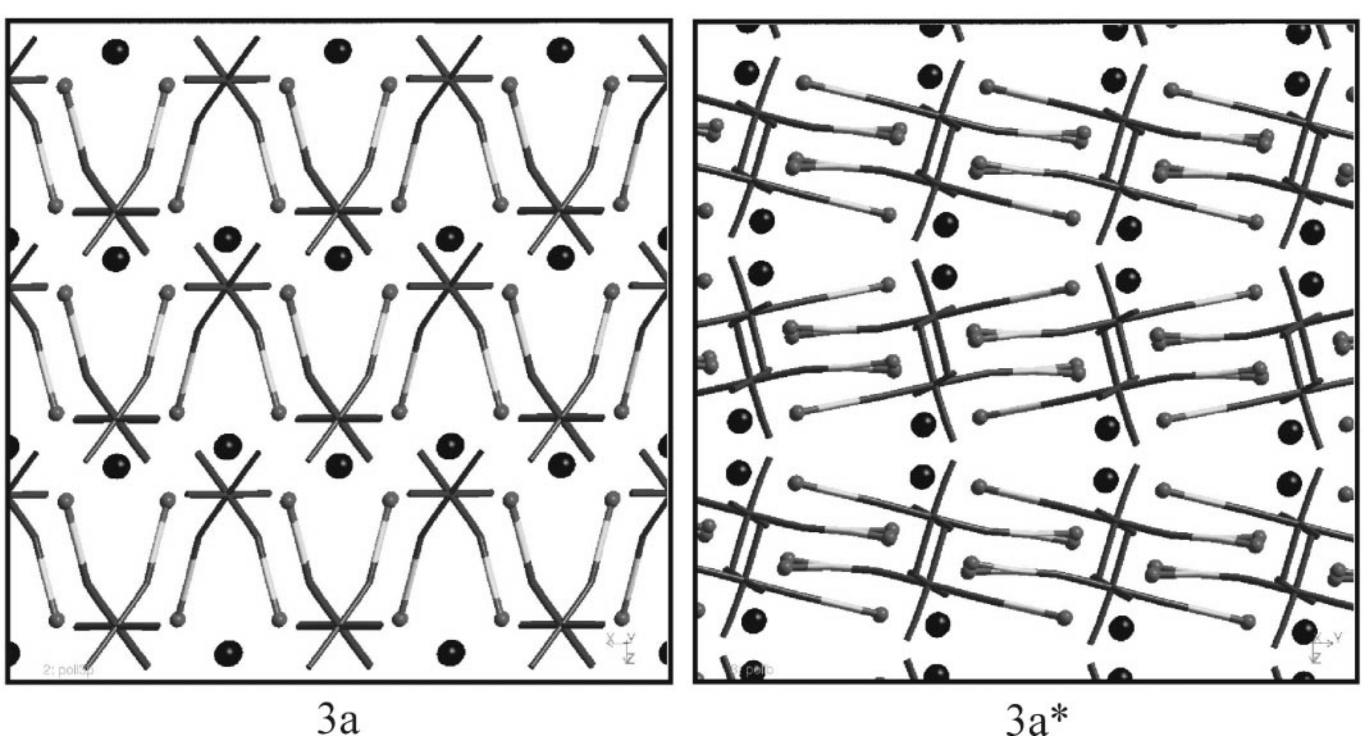

FIG. 2. Views down *b* of a fragment of **3a** and down *c* of a fragment of **3a***. Large spheres represent the (centers of) $n\text{Pr}_4\text{N}^+$ ions, and smaller spheres oxygen atoms (of H_2O molecules). Sn-bonded CH_3 groups and other H atoms have been omitted for clarity. (Sn atoms: grey).

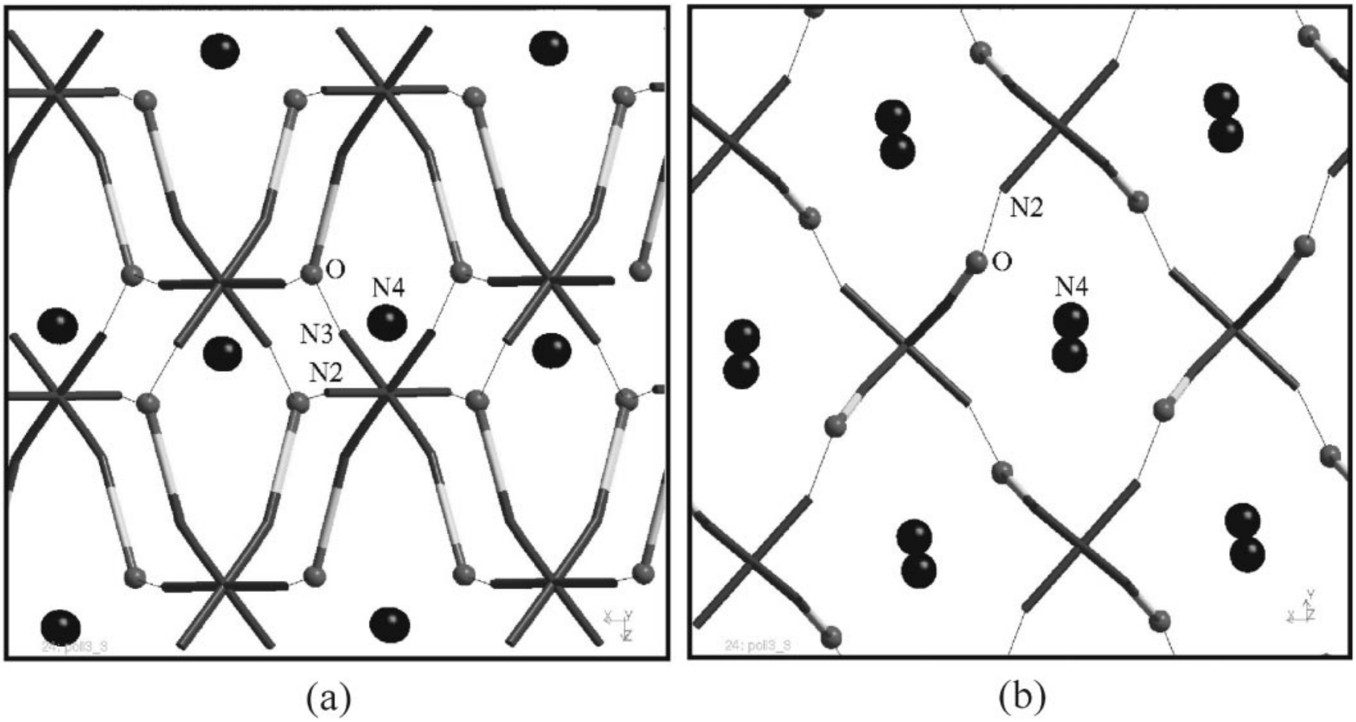

FIG. 3. Views down *b* (a) and *c* (b), respectively, of fragments of **3a**. Faint straight lines indicate O–H ⋯ N hydrogen bonds. For further explanations see the caption of Fig. 2.

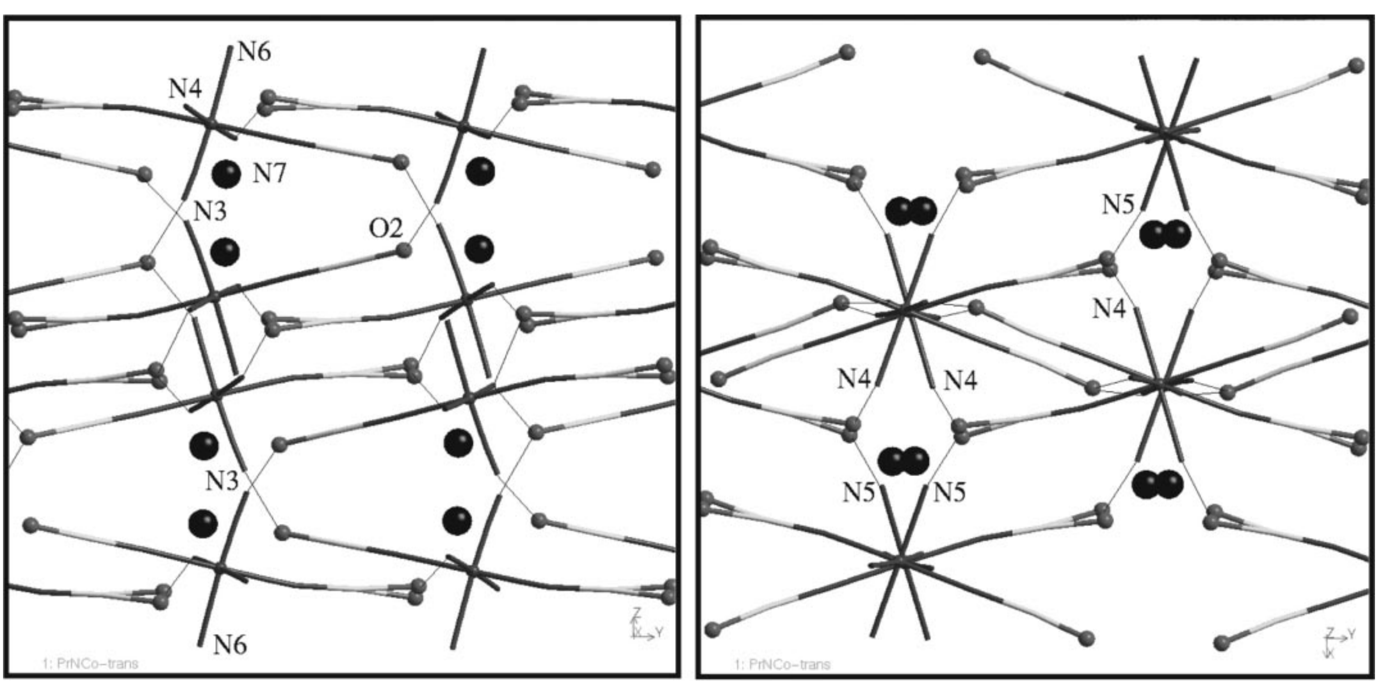

FIG. 4. (a) Perspective along *a* (horizontal axis: *b*), and (b) along *c* (horizontal axis: *a*) of **3a***, indicating O–H ⋯ N hydrogen bonds as faint straight lines. For further explanations see the caption of Fig. 2.

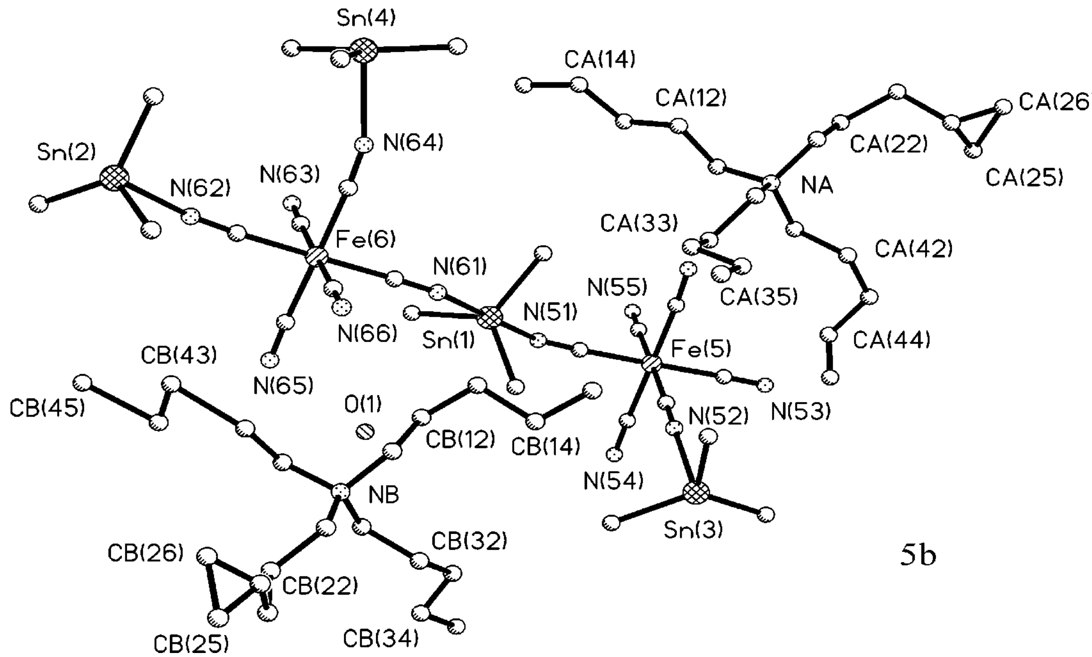

FIG. 5. Asymmetric unit of **5b**. Only the cyanide N atoms N55, N56, N65, and N66 are terminal. Moreover, Sn1, Sn2, Sn3, and Sn4 carry three crystallographically different methyl groups each. For the Sn–N connectivities in total see Table 3. The second number in the designation of each *n*-pentyl carbon refers to its position (i.e. 1 = α, 2 = β, etc.).

cis-oriented CN ligands that are not coordinated to a tin atom.

The values of all C(Me)–Sn–N angles of **5b** scatter closely around 90°, and none of the N–Sn–N angles deviates notably from 180° (Table 5). Moreover, all Sn–N bond distances adopt values very close to 2.31 Å, whereas all Sn–N–C angles are notably smaller than 180° and vary significantly. This feature and the *cis*-orientation of the two nonbridging CN ligands admit a *three*-dimensional expansion of the negatively charged, polymeric framework. Both the nPen$_4$N$^+$ ions and the H_2O molecules are encapsulated in suitable cavities of this 3D framework.

TABLE 5
Selected Interatomic Distances (Å) and Angles (°) of 5b

Sn1–C1i	2.104(4)–2.113(4)	N51–Sn1–N61	179.41(9)
Sn2–C2i	2.114(4)–2.122(4)	N62–Sn2–N63	178.78(13)
Sn3–C3i	2.109(4)–2.122(4)	N52–Sn3–N53	177.52(12)
Sn4–C4i	2.111(4)–2.115(5)	N54–Sn4–N64	179.63(14)
Sn1–N51	2.329(3)	Sn1–N51–C51	147.7(3)
Sn1–N61	2.329(3)	Sn1–N61–C61	152.8(3)
Sn2–N62	2.294(3)	Sn2–N62–C62	161.2(3)
Sn2–N63	2.341(3)	Sn2–N63–C63	162.4(3)
Sn3–N52	2.329(3)	Sn3–N52–C52	170.2(3)
Sn3–N53	2.306(3)	Sn3–N53–C53	153.2(3)
Sn4–N64	2.313(3)	Sn4–N64–C64	161.4(3)
Sn4–N54	2.309(3)	Sn4–N54–C54	161.9(3)

Note. The Sn–C distances are maximum and minimum values (i = 1–3).

In contrast to **3a**, **3a***, and **4b**, the H_2O guest molecule of **5b** is anchored only via O–H $\cdots$ N hydrogen bonds to the N65 atoms of two different chains. The O $\cdots$ N65 distances of **5b** are notably longer than the O $\cdots$ N distances found in **3a**, **3a***, and **4b**, where the H atoms seem to be better activated ("acidified") for bridging owing to concomitant $H_2O \rightarrow Sn$ coordination. In Table 6 all C $\cdots$ NC distances between methylene carbon atoms of the nPen$_4$N$^+$ ions of **5b** and cyanide N atoms are listed. As usual (9), exclusively nitrogen atoms of terminal cyanide ligands are involved, the shortest distances resulting mostly from interactions with α-CH$_2$ groups (designated in Table 6 as CA*i*1 or CB*i*1 with i = 1–4). In fact, most of the positive charge of a R_4N^+ ion is usually distributed over its α-CH$_2$ groups (rendering these hydrogen atoms particularly "acidic"), although from a purely geometrical point of view the β-, γ-, and δ-CH$_2$ groups should approach relevant atoms of adjacent anions more readily. According to Table 6, each of the nitrogen atoms N55, N56, and N66 seems to be involved in two C–H $\cdots$ N hydrogen bonds with C $\cdots$ N distances between 3.30 and 3.45 Å, while only for N65 the two distances range between 3.51 and 3.58 Å.

The formation of wide channels in the lattice of **5b** with approximately rectangular cross sections of 1 × 2 nm is visualized in Fig. 6. These channels clearly exceed in size those of the R_4N^+-free 3D framework **2** (Fig. 6d), but match reasonably well with the nBu$_4$N$^+$-containing channels of the lattice of **1b** (7). However, while in **1b** each nBu$_4$N$^+$ ion resides in one singular channel, the *n*-pentyl groups of the

TABLE 6
Interatomic O ··· N and C ··· N distances (in Å) of 5b

O ··· N65	2.967(7)	O ··· N65′	2.980(7)
N55 ··· CA12	3.779(6)	**N65 ··· CB31**	**3.513(7)**
N55 ··· CA21	**3.410(6)**	N65 ··· CB33	3.865(11)
N55 ··· CA22	3.603(6)	N65 ··· CB34	3.874(13)
N55 ··· CA23	3.653(7)	**N65 ··· CB41**	**3.575(7)**
N55 ··· CB11	**3.374(6)**	N65 ··· CB42	3.929(19)
N55 ··· CB21	**3.326(6)**	N65 ··· CB43	3.750(12)
		N65 ··· CB44	3.718)16)
N56 ··· CA11	**3.365(6)**	**N66 ··· CA21**	**3.434(6)**
N56 ··· CA11′	**3.705(6)**	**N66 ··· CA31**	**3.391(6)**
N56 ··· CA12	3.702(7)	N66 ··· CA42	3.950(8)
N56 ··· CA13	3.511(7)	**N66 ··· CB11**	**3.665(7)**
N56 ··· CA22	3.870(7)	N66 ··· CB12	3.605(7)
N56 ··· CA41	**3.298(7)**	N66 ··· CB13	3.614(7)
N56 ··· CA44	3.880(11)	N66 ··· CB42	3.554(10)

Note. A and B refer to the nonequivalent $n\mathrm{Pen}_4\mathrm{N}^+$ ions, and the numbers of the C atoms to the different pentyl groups (first) and to the position of the CH_2 group (second), respectively. Boldface letters indicate potential interactions involving α–CH_2 groups.

$n\mathrm{Pen}_4\mathrm{N}^+$ ions of **5b** are spread out through the channel walls. This more composite-like nature of **5b** is depicted in Fig. 7.

X-Ray Powder Diffractometric (XRD) Studies

The simulated XRDs of "crystalline" **3a**, **3a***, and **5b** based on data available from the single-crystal X-ray studies of these compounds were compared with the corresponding experimental diffractograms (of "bulk" material) as well as with the likewise experimental XRD's of **5b***, **5a**, and **5a***. Satisfactory agreement is found for the XRDs of crystalline and bulk **3a** (Fig. 8) and for crystalline **5b**, bulk **5b** and bulk **5a**, respectively (Fig. 9). In contrast, the simulated XRD of **3a*** had to be modified slightly (see Experimental) to arrive at better agreement with the experimental XRD (Fig. 10). These findings in total confirm that bulk probes of **3a** and **5a** are isostructural with crystalline **3a** and **5b**, respectively, and justify therefore the examination of the solid-state NMR results for the bulk materials strictly in terms of the respective asymmetric units deduced from single-crystal X-ray crystallographic work. In the case of **3a***, where the quality of the single crystal was undoubtedly excellent, too, the quality of the bulk material is likely to differ slightly from that of (so far unavailable) finely ground single crystals (vide infra).

Multinuclear (^{13}C, ^{15}N, ^{59}Co, ^{119}Sn) Solid-State Magnetic Resonances Studies of **3a**

A collection of all NMR data of relevance for **3a** is given, along with corresponding surveys for **3a*** and **5a**, in Table 7. The NMR results appear to reflect the disorder of the tin-bonded methyl carbon atoms of the *cis*-configured $[Co(CN)_4(CNSnMe_3OH_2)_2]^-$ anion of **3a** (vide supra) more clearly than the crystallographic findings. Thus, two distinct ^{119}Sn centerbands appear (Fig. 11), each of which could be attributed to a tin atom associated with one of the two sets of methyl carbon atoms found crystallographically. In the ^{13}C NMR spectrum (Fig. 12), these two sets of methyl carbon atoms give rise to two equally intense singlets at $\delta_C = 1.2$ and 2.2 ppm accompanied by weak satellite doublets due to the presence of ^{117}Sn and ^{119}Sn nuclei. The appearance of just two ^{13}C(Me) signals at room temperature, in spite of the existence of six crystallographically nonequivalent methyl carbon atoms, is explained by rapid rotation of the two different Me_3Sn groups about their N–Sn–O axes. According to earlier findings (9, 18), this kind of motion has a low activation barrier, as no splitting of the ^{13}C resonances was observed for **3a** down to a temperature of -80°C. The disorder of the Me_3Sn groups is, moreover, reflected by the clear doublet character of one of the three expected (in view of the asymmetric unit of **3a**; see Fig. 1) ^{15}N resonances (see Fig. 13 and Table 7). Indeed, the relative intensities visible in Fig. 13 suggest that the peak at $\delta_N = -95$ ppm is a composite, with the total intensity for one nitrogen site together with a doublet component for a second site (with its companion at $\delta_N = -99$ ppm). Two ^{15}N resonances appear in the spectral range characteristic of virtually nonbridging CN ligands (9), while the quasi-doublet is found at lower frequency, which would correspond well with an assignment to tin-coordinated (i.e., bridging) CN ligands.

The $\delta(^{119}Sn)$ data match well with the chemical ^{119}Sn shift values reported for tbp-configured N–Sn(Me_3)–O fragments in negatively charged frameworks (9, 15a). Each signal is split into an unsymmetrical triplet, clearly indicating coupling to a single ^{14}N nucleus (thus confirming the existence of an N–Sn–O fragment). The unsymmetrical nature of the triplet arises from the well-known second-order effects of coupling to a quadrupolar ($I = 1$) nucleus (19). Similarly, ^{119}Sn quintets have been observed in the spectrum of **2a** which contains N–Sn(Me_3)–N fragments (14). On the other hand, a sample of **3a** with ^{15}N-enriched cyanide ligands (98%) displayed two ^{119}Sn *doublets* (see insert of Fig. 11), in accordance with $I = \frac{1}{2}$ for the ^{15}N nucleus.

As usual, the large electric quadrupole moment of the ^{59}Co nucleus prevents the resolution of the cyanide ^{13}C resonance into the expected three to four signals; thus, some fine structure is visible for **3a** enriched in ^{15}N, but it cannot be fully interpreted. The ^{59}Co nucleus itself gives rise to a single band (Fig. 14) centered around -30 ppm, which lies in the same region as the complex ^{59}Co resonances of **4a** (9). The shape of the ^{59}Co resonance is typical for that of a quadrupolar nucleus with second-order-features. It could be simulated satisfactorily (20) for a quadrupolar coupling

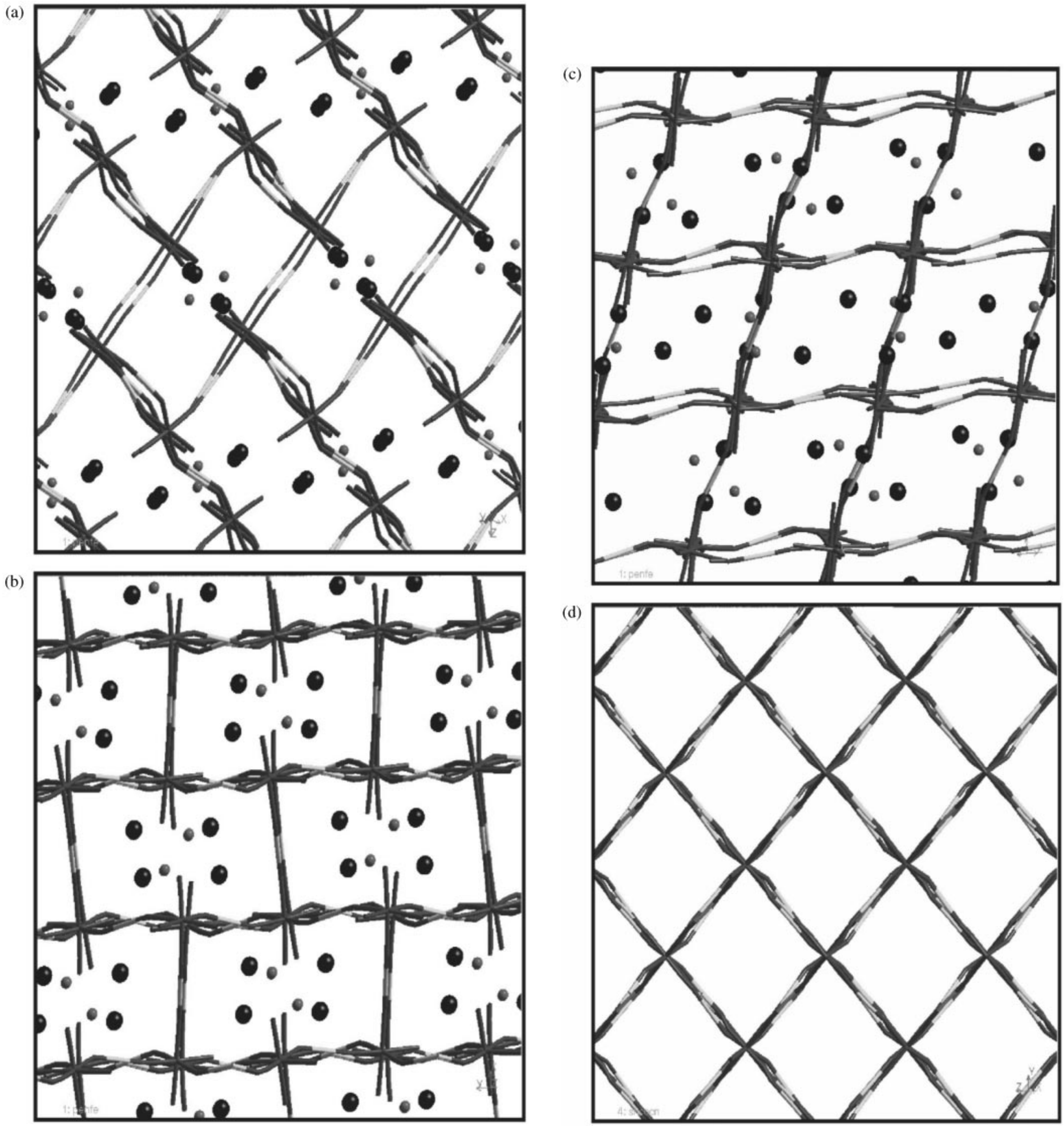

FIG. 6. Views down *ab* (a), *c* (b), and *bc* (c), respectively, of fragments of **5b**. Alkyl groups (Me, *n*Pen) and other H atoms are omitted for clarity. For better comparison, (d) presents the view down *ac* of **2** (12). For further explanations see the legend of Fig. 2.

constant of 8 MHz and an asymmetry factor of 0.6. The true chemical shift is $\delta_{Co} = -8$ ppm.

The NMR results do not reflect the slight disorder of the nPr_4N^+ ion (vide supra). Just one sharp ^{15}N singlet appears in the correct δ-range (Table 7), and three rather broad, but comparatively symmetrical ^{13}C resonances can be ascribed to the α-, β-, and γ-carbon atoms. The crystallographically suggested disorder of the tin-bonded methyl groups of **3a** is

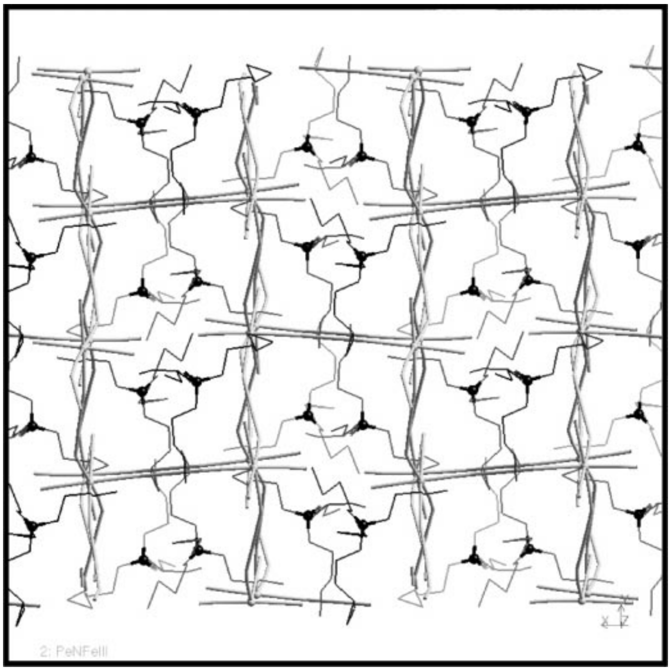

FIG. 7. Arrangement of the $n\mathrm{Pen}_4\mathrm{N}^+$ ions (tender lines) in the host framework of **5a** (view along *c*).

NMR time scale. Instead of two ^{119}Sn, six ^{15}N, and two ^{13}C signals (for rapidly rotating Me_3Sn units), respectively, each nucleus gives rise to no more than one signal. However, it is clear that the effective *local* symmetry is higher than the crystallography suggests, especially in the presence of Me_3Sn rotation, so the experimental observations are not surprising. As for **3a**, the ^{119}Sn centerband for **3a*** is found in the δ-range characteristic of tbp-configured N–Sn(Me_3)–O fragments in a negatively charged framework (9). The only cyanide ^{15}N signal to be discriminated from the rather noisy base line appears at relatively high frequency, where the *four* crystallographically nonequivalent, terminal cyanide ^{15}N nuclei should resonate. However, no signal characteristic of Sn-coordinated (i.e., bridging) nitrogen is found, at least for the presently available sample nonenriched in ^{15}N. The methyl ^{13}C signal is comparatively broad and unsymmetrical and likely to be resolvable on cooling. The ^{59}Co NMR spectrum of **3a*** differs substantially from that of **3a** (Fig. 14), while still consisting of a single band influenced by second-order quadrupolar effects. A simulation of the ^{59}Co spectrum of **3a*** shows that the true chemical shift is $\delta_{\mathrm{Co}} = -46$ ppm. The calculation also reveals that the *trans*-configured cobalt complex has a significantly higher quadrupolar coupling

well corroborated by the ^{119}Sn, ^{15}N-, and ^{13}C-solid-state NMR spectra. These results might even raise the question if the crystal structure of **3a** would more correctly be described by a space group still less symmetrical than $P2_12_12$. However, according to an attempted Rietveld analysis of the experimental XRD of **3a**, the lattice parameters *a*, *b*, and *c* remain the same as given in Table 1. The very satisfactory agreement of the experimental with the simulated XRD of **3a** (Fig. 8) suggests that only a more powerful X-ray diffractometer than the one used could possibly help deciding if any more reflections than those so far detected might be of relevance. The solid-state NMR results undoubtedly confirm that two nonequivalent Me_3Sn fragments are reality, no matter whether they are arranged in a more regular or random order (see also note added in proof).

Multinuclear (^{13}C, ^{15}N, ^{59}Co, ^{119}Sn) Solid-State Magnetic Resonance Spectra of **3a***

As far as the ^{15}N and ^{13}C resonances of the $n\mathrm{Pr}_4\mathrm{N}^+$ ion and the cyanide carbon atoms are concerned, the spectra of **3a*** and **3a** do not differ significantly. Only the (γ-) methyl carbon atoms of **3a*** display, in good agreement with the asymmetric unit, four distinct lines (Table 7). Although the asymmetric unit predicts for the *trans*-configured anion of **3a*** more ^{119}Sn-, ^{15}N-, and ^{13}C-resonances than for the *cis*-isomer, the reverse is found experimentally, suggesting here, inter alia, some "molecular" mobility rapid on the

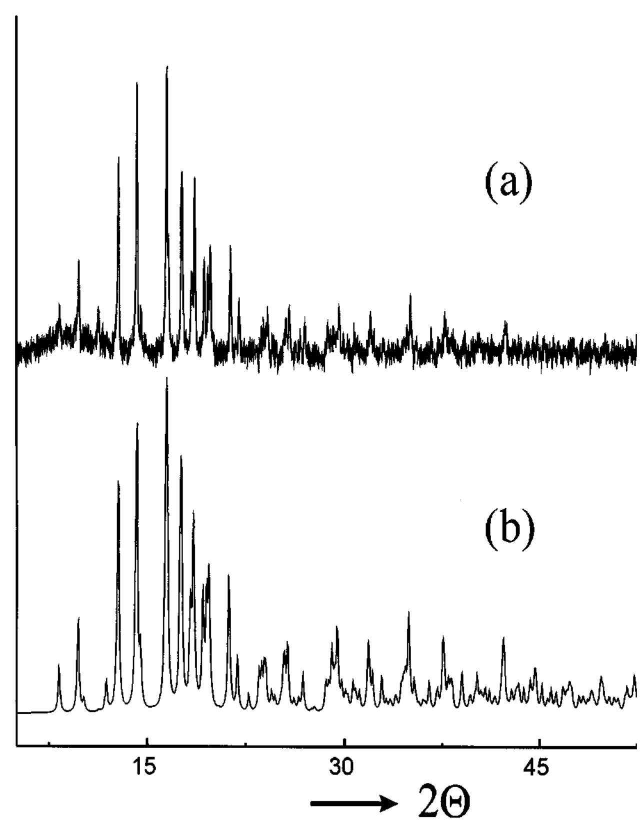

FIG. 8. Experimental (a) and simulated (b) XRDs of **3a**.

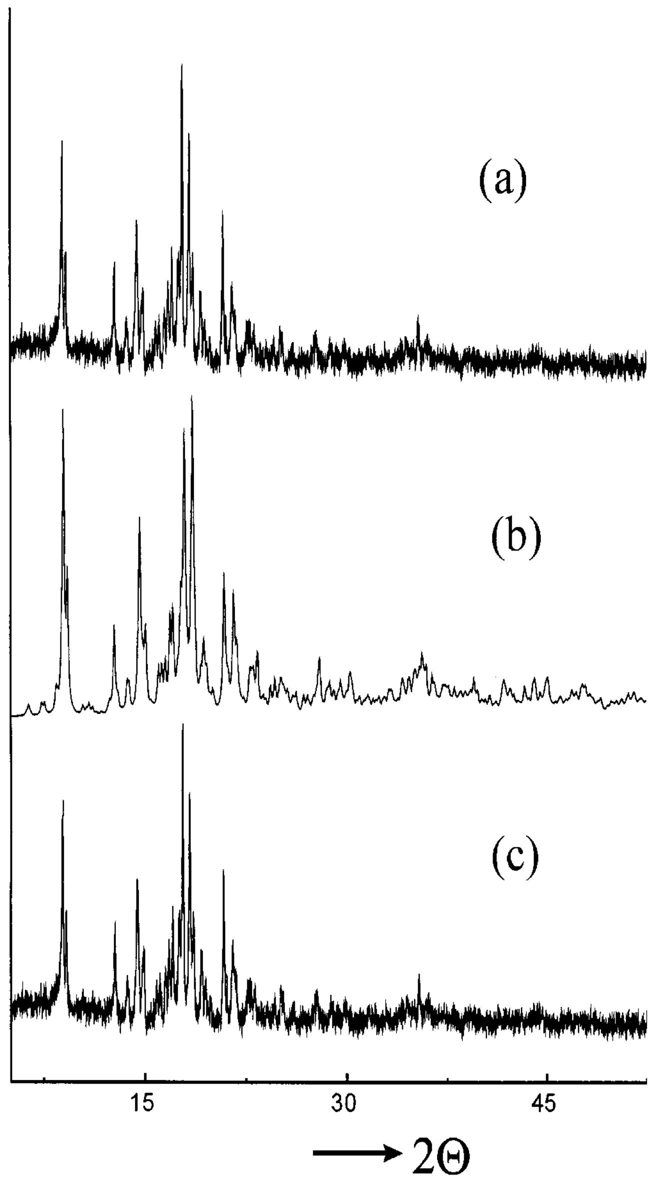

FIG. 9. Comparison of the experimental XRD of **5a** (a) with the simulated (b) and experimental (c) XRDs of **5b**.

constant (of ca. 13 MHz) than **3a**, but an asymmetry factor of zero. While the latter finding is plausible owing to the quasi-rotational local symmetry of the anion (see Fig. 1), the large difference of the $\delta(^{59}Co)$ values of **3a*** and **3a** has no simple explanation, though the strongly axial character of the bonding may supply some rationalization.

Multinuclear (^{13}C, ^{15}N, ^{59}CO, ^{119}SN) Solid-State Magnetic Resonance Spectra of **5a**

In excellent agreement with the crystal structure of this host/guest assembly, only ^{119}Sn resonances typical of N–Sn(Me_3)–N fragments (with δ-values more negative than − 100 ppm) are found (Fig. 11). They are, however, devoid of any multiplet patterns. Likewise, ^{15}N resonances with δ-values typical of both bridging *and* terminal cyanide N atoms occur (Fig. 13). Interestingly, as expected owing to the *absence* of Sn ← O–H ⋯ NC hydrogen bonds in **5b** (vide supra), the terminal ^{15}N nuclei of **5a** resonate at higher frequencies (− 75 ± 3 ppm) than the likewise virtually terminal ^{15}N nuclei of **3a** and **3a*** (− 95 ± 3 ppm). The latter nitrogen atoms are in fact involved in notable Sn ← O–H ⋯ NC bonding (vide supra). A corresponding rationale for the discrimination of the ^{15}N shifts had already emerged for **4a** (9). Two sharp ^{15}N resonances appear

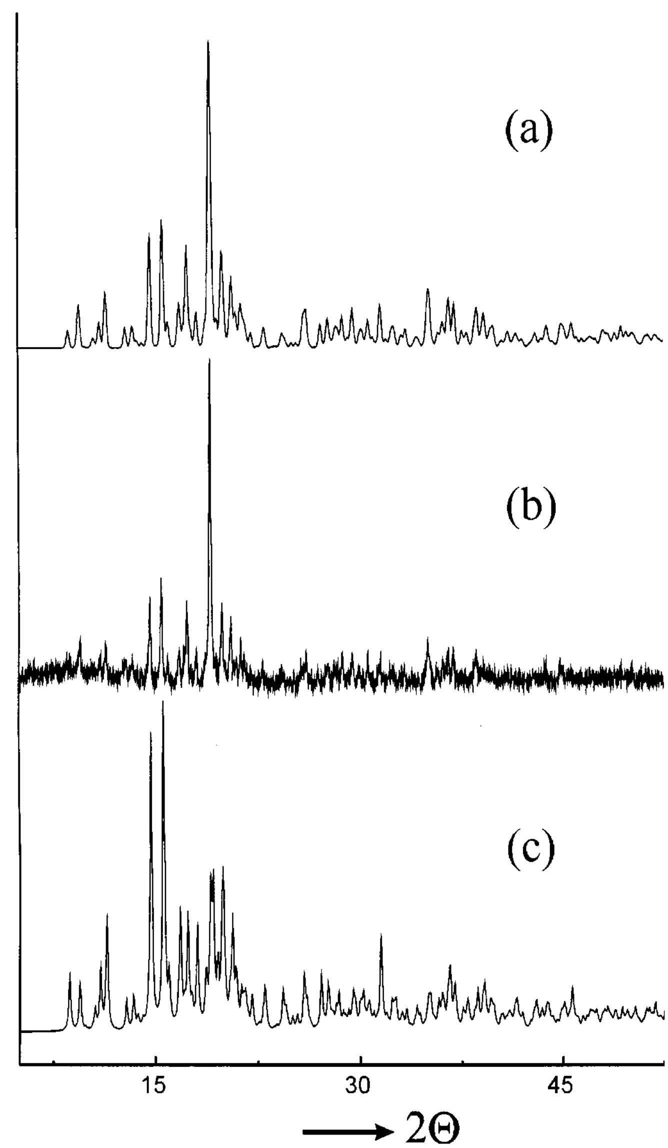

FIG. 10. XRDs of **3a***: (a) Improved simulation (see the text), (b) bulk sample, (c) standard simulation.

TABLE 7
NMR Parameters for Compounds 3a, 3a*, and 5a

Nucleus	Environment/ Position	Samples 3a	3a*	5a
^{119}Sn	Me_3Sn	− 75[a]	− 79	− 106
		− 61[b]		− 124
				− 129
^{15}N	CN[c]	− 95	− 92	− 73
		− 98		− 78
		− 125.0		− 120, − 123,
		− 125.4		− 124, − 125
	R_4N	− 308	− 309	− 309
				− 310
^{13}C	CN	ca. 130[d]	ca. 130[d]	ca. 136, 121
	α-CH_2	60.1	ca. 61[e]	59, 58
	β-CH_2	15.8	16.5	31 to28
	γ-$CH_{3/2,}$	12.5	13.6, 12.4,	24 to 20
			11.6, 11.0	
	δ-CH_2			24 to 20
	ε-CH_3			17 to 15
				15.8, 15.5
	Me_3Sn	2.2[f]	ca. 0.5[e]	1.2[h], 0.7[h],
		1.2[g]		0.5[h], 0.3[h]
^{59}Co		-8	-46	-91[i]

[a] $|J_{SnN}| = 170$ Hz (for ^{15}N) from measurements on a ^{15}N-enriched sample.
[b] $|J_{SnN}| = 134$ Hz (for ^{15}N) from measurements on a ^{15}N-enriched sample.
[c] The relative integrated intensities of the three bands are 55 : 20 : 25 (i.e., within experimental error of 3 : 1 : 1), with the last mentioned representing the doublet at $\delta_N = -125.0/-125.4$ ppm.
[d] Complex multiplet.
[e] Broad singlet.
[f] $|J_{SnC}| = 554$ Hz.
[g] $|J_{SnC}| = 546$ Hz.
[h] $|J_{SnC}| =$ ca. 570 Hz for each site.
[i] Broad singlet band center (true chemical shift will be influenced by second-order quadrupolar effects)

around − 309 ppm for **5a**, in good agreement with the presence of two crystallographically nonequivalent nPr$_4$N$^+$ ions.

Instead of four (asymmetric unit), only three ^{119}Sn lines are found, although the line at − 124 ppm seems to be twice as intense as each of the other two singlets. Likewise, only two ^{15}N signals (instead of four) appear around − 75 ppm and only four (instead of eight) around − 122 ppm. However, the signal at − 73 ppm is about three times as intense as the signal at − 78 ppm, and each of the lines at − 124 and − 123 ppm is notably more intense than, e.g., the well-isolated signal at − 120 ppm (see Fig. 13). An overlapping of certain lines is not unreasonable, since e.g. for the atoms N51 and N61 equal Sn–N distances and very similar Sn–N–C angles are found (Table 5). Although the crystal structure of **5b** involves two nonequivalent Fe atoms, the ^{59}Co NMR spectrum of its homolog **5a** displays only one, albeit extremely broad, resonance centered at − 91 ppm (Fig. 14). The quadrupole coupling constant is probably similar to or less than that of **3a***, but the true chemical shifts are not obtained, nor can the probably two nonequivalent cobalt atoms of **5a** be discriminated.

The ^{13}C NMR spectrum of **5a** displays, first of all, four centerbands between 1.3 and 0.2 ppm which could be assigned to the four nonequivalent Me_3Sn groups present, provided that, as usual, rapid rotation about the N–Sn–N axes takes place. Two slightly unsymmetrical centerbands of

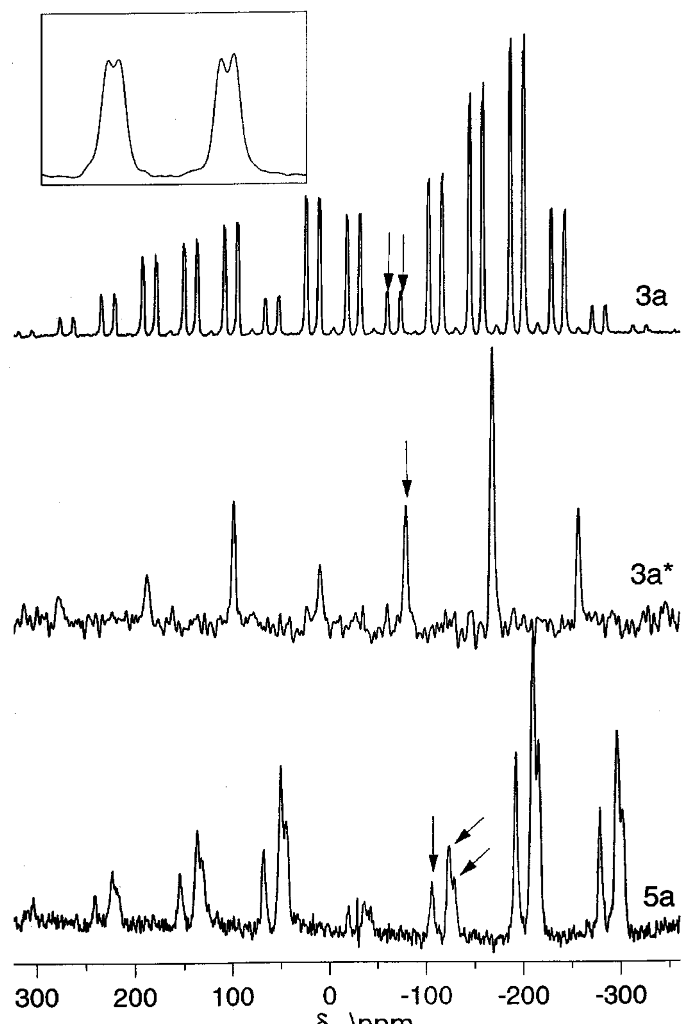

FIG. 11. Tin-119 NMR spectra obtained by cross polarization with flip-back. Centerbands are shown by arrows. See inset region for an enlarged view of the centerbands for **3a** with ^{15}N enriched (98) CN ligands. Conditions: **3a**: Contact time, 10.0 ms; acquisition time, 20.0 ms; recycle delay, 5.0 s; spin rate; 7680 Hz; number of transients, 65,536. **3a***: Contact time, 1.0 ms; acquisition time: 20.0 ms; recycle delay, 5.0 s; spin rate, 9940 Hz; number of transients, 32768. **5a**: Contact time, 10.0 ms; acquisition time, 9.9 ms; recycle delay, 2.0 s; spin rate, 9830 Hz; number of transients, 12,440.

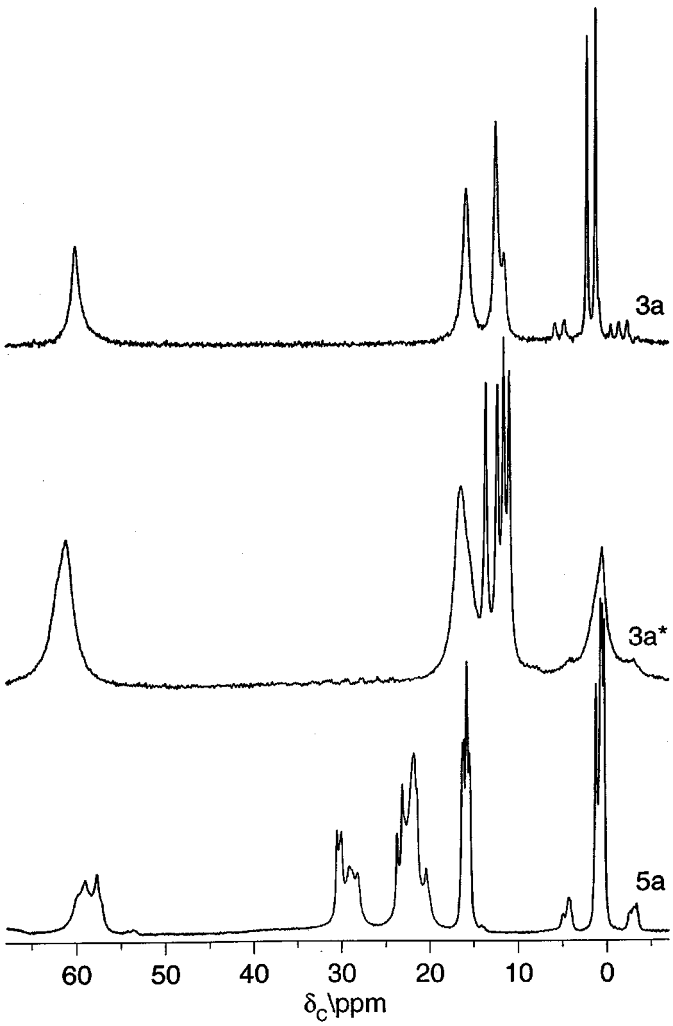

FIG. 12. Carbon-13 NMR spectra obtained by cross-polarization with flip-back. Conditions: **3a**: Contact time, 3.00 ms; acquisition time, 89.6 ms; recycle delay, 2.0 s; spin rate; 4800 Hz; number of transients, 332. **3a***: Contact time, 1.00 ms; acquisition time, 60.2 ms; recycle delay, 5.0 s; spin rate, 4000 Hz: number of transients, 11376. **5a**: Contact time, 10.00 ms; acquisition time, 80.0 ms; recycle delay; 2.0 s; spin rate, 4000 Hz: number of transients, 11,808.

different intensities at 136 and 121 ppm can be correlated with cyanide carbon atoms of terminal and bridging CN ligands, respectively. Four signals of different intensities between 15.5 and 16.5 ppm can be ascribed to the eight nonequivalent ε-carbon atoms (terminal methyl groups) of the two $n\mathrm{Pen}_4\mathrm{N}^+$ ions. One rather broad resonance between 20 and 24 ppm (with no more than four distinct peaks) is probably due to the γ- and δ-CH_2 carbon atoms, and a likewise broad resonance between 28 and 31 ppm (with four distinct peaks) to the β-CH_2 carbons. The α-methylene carbon atoms resonate between 56 and 62 ppm (two distinct peaks and several shoulders).

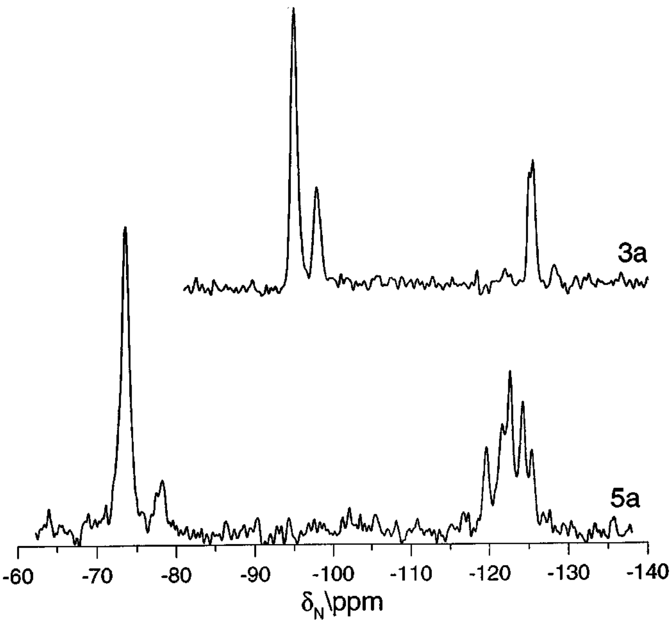

FIG. 13. Nitrogen-15 NMR spectra of compounds **3a** and **5a** (centerbands only) obtained by cross-polarization with flip-back. Conditions: **3a**: Contact time, 20.0 ms; acquisition time, 100.2 ms; recycle delay, 5.0 s; spin rate, 4000 Hz; number of transients, 11,364. **5a**: Contact time, 10.0 ms; acquisition time, 80.0 ms; recycle delay, 2.0 s; spin rate; 4500 Hz; number of transients, 36,620.

CONCLUSIONS

Simple quaternary ammonium ions R_4N^+ with $R = n\mathrm{Pr}$, nBu (9) and nPen have turned out to be very efficient cleavage agents, and concomitant "structure directors", respectively, for the preparation of the host/guest systems $[(R_4\mathrm{N})(\mathrm{Me}_3\mathrm{Sn})_2M(\mathrm{CN})_6\cdot z\mathrm{H}_2\mathrm{O}]$ according to Equation [2]. In contrast, R_4N^+ ions with R = Me and Et, as well as with $R = n\mathrm{Hex}$ (and probably longer n-alkyl chains, too), do *not* react with **2**. Interestingly, coprecipitation in the presence of a *reactive* R_4N^+ ion (see Eq. [3]) leads to the same type of host/guest assembly as Me_3Sn-exchange (Eq. [2]), whereas in the presence (*and* absence) of "nonreactive" R_4N^+ ions exclusively the long-known (12) *super*-Prussian blue derivative **2** precipitates.

While several molecular recognition experiments of tetraalkylammonium ion by *molecular* receptors have been described (21), efficient R_4N^+-receptors consisting of infinite 3D frameworks have so far not explicitly been mentioned, although some of the numerous but quite frequently ignored, as-synthesized zeolites containing R_4N^+ guests (1) could provide suitable examples. The efficient discrimination between, e.g., $n\mathrm{Et}_4\mathrm{N}^+$ and $n\mathrm{Pr}_4\mathrm{N}^+$ ions by the 3D host described in this contribution is quite remarkable. Another unexpected feature is the very different structure-directing behavior of $n\mathrm{Pr}_4\mathrm{N}^+$ and $n\mathrm{Pen}_4\mathrm{N}^+$ ions. While the former is

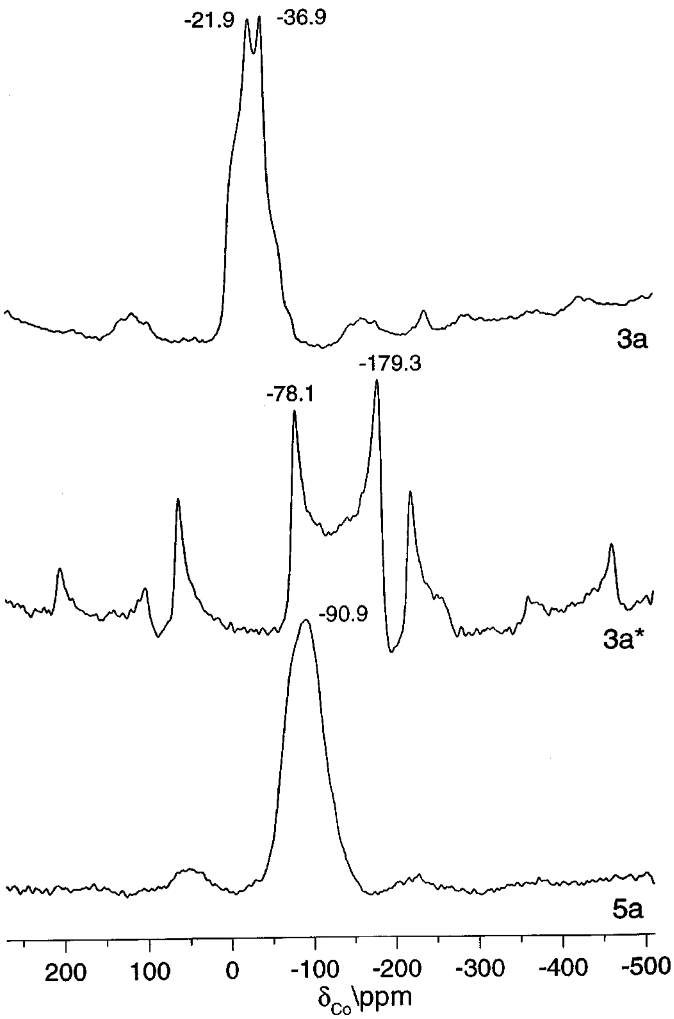

FIG. 14. Cobalt-59 NMR spectra. Conditions: **3a**: Direct polarization; pulse duration,1.0 μs; acquisition time, 3.0 ms; recycle delay, 0.5 s; spin rate, 4000 Hz; number of transients, 2000. **3a***: Direct polarization; pulse duration, 1.0 μs; acquisition time, 3.0 ms; recycle delay, 0.5 s; spin rate, 10040 Hz; number of transients, 100,000. **5a**: Direct polarization; pulse duration, 1.0 μs; acquisitions time, 3.0 ms; recycle delay, 0.5 s; spin rate, 9310 Hz; number of transients, 2500.

able to generate two isomeric 3D frameworks containing only $Sn \leftarrow OH_2 \cdots NC$ connecting units, the latter admits exclusively the formation of infinite [*M*–CN–Sn–NC] chains. Interestingly, the nBu$_4$N$^+$ ion has been shown (9) to lead to the particularly complex 3D framework **4b** involving both $Sn \leftarrow OH_2 \cdots NC$ connectors and infinite chains. In zeolite chemistry, the application of the nPr$_4$N$^+$ ion as a structure director has not led to exceedingly unexpected results, although the nPr$_4$N$^+$ ion is most essential for the hydrothermal synthesis of the zeolite ZSM-5 which is quite important for technical applications (22,23).

On the other hand, the two so far unprecedented isomeric $[Co(CN)_4(CNSnMe_3OH_2)_2]^-$ anions present in **3a** and **3a*** seem to owe their stabilization essentially to the formation of the specific 3D frameworks described above. This situation is reminiscent of the stabilization of other "elusive" anions in host/guest systems containing likewise R_4N^+ guests (R = e.g., nPr) and, e.g., hosts built up of urea and the elusive "allophanate" anion (24).

A survey of the variety of reaction products resulting according to Eqs. [2] and [3] with the different R_4N^+ ion is given in Table 8. Interestingly, both the number of H_2O molecules (z) and the number of terminal cyanide ligands per $\{M(CN)_6\}$ unit passes a maximum value as the chain length of R increases from one to six atoms. The uptake of R_4N^+ ions by the polymeric framework seems to be coupled with that of H_2O, leaving room for spectulation on any favorable interaction of H_2O and R_4N^+ already in aqueous solution. The presence of terminal cyanide ligands is important for an anchoring of the H_2O and R_4N^+ guests via hydrogen bonding. Although any quantitative assessment seems to be premature, it might be justified arguing that these hydrogen bonds in total presumably help overcompensating the deficiency in bonding energy owing to the replacement of two, three or even four $N \rightarrow Sn$ bonds by energetically less efficient $O \rightarrow Sn$ bonds during the formation of **3a**, **4a** and **5a**, respectively, from **2a** according to Eq. [2] (vide supra).

TABLE 8
Structural Variation of a $[(R_4N)_x(Me_3Sn)_{3-x}M(CN)_6 \cdot zH_2O]$ Assembly, Steered by the Length of the Group *R* Present in the R_4N^+ Ion (for *M* = Co and Fe)

R	Product No.	*x*	*z*	[*M*–CN–Sn–NC] chains present	$Sn \leftarrow OH_2 \cdot\cdot NC$ bridges present	No. of terminal CN ligands per *M*	Comment
Me	**2**	0	0	Yes	No	0	[a]
Et	**2**	0	0	Yes	No	0	[a]
*n*Pr	**3**	1	2	No	Yes	4	[b]
*n*Pr	**3***	1	2	No	Yes	4	[c]
*n*Bu	**4**	1	1	Yes	Yes	3	[d,e]
*n*Pen	**5**	1	0.5	Yes	No	2	[f]
*n*Hex	**2**	0	0	Yes	No	0	[a]

[a] Exclusive formation (or persistence) of **2** = $[(Me_3Sn)_3M(CN)_6]$
[b] As isomer **3a** with cis-$[Co(CN)_4(CNSnMe_3OH_2)_2]^-$ anion.
[c] As isomer **3a*** with *trans*-$[Co(CN)_4(CNSnMe_3OH_2)_2]^-$ anion.
[d] With both finite and infinite [*M*–CN–Sn–NC] chains.
[e] Various kinds of $Sn \leftarrow OH_2 \cdots CN$ hydrogen bridges are present
[f] 3D-framework with channels of nanometer-sized (ca. 1 × 2 nm) cross section.

As in earlier studies (5, 7–9), the combination of X-ray crystallography and multinuclear CPMAS solid state NMR spectroscopy has again proved to be very helpful. Apart from the mutual support and control, respectively, of deductions resulting just from one of these methods, sufficient experience has meanwhile been accumulated to draw significant conclusions from multinuclear CPMAS solid state magnetic resonance results alone.

Actually, the presence of [Co–CN–Sn(Me_3)–NC] chains, and the absence of $Me_3Sn \leftarrow OH_2$ bonds, in the architecture of **5b** had been correctly deduced before the X-ray crystallographic results were available. Special attention should also be paid to the notable sensitivity of the ^{59}Co bandshape of the $\{Co(CN)_6\}$ unit in response to even subtle changes of its environment.

ACKNOWLEDGMENTS

This work was supported by the Deutsche Forschungsgemeinschaft (Joint Project: Nanoporous Crystals) and the Fonds der Chemischen Industrie. The extensive CPMAS NMR work was supported by the UK EPSRC (through the National Solid-State Magnetic Resonance Service based at Durham). We thank Professor H. J. Jakobsen for a copy of the computer simulation program for quadrupolar bandshapes.

Note added in proof (Febr. 22, 2000). (a) Since the manuscript of this paper has been submitted, we have become aware of recent experiments dealing with the successful reaction of neat SiO_2 with (R_4N)OH to afford large single crystals of "as-prepared" zeolites. This mode of reaction parallels the reaction of a polymeric metal cyanide with R_4N^+ ions (cf. the Introduction). See S. Shimizu and H. Hamada, *Angew. Chem.* **111,** 2891 (1999); *Angew. Chem. Int. Ed. Engl.* **38,** 2725 (1999).

(b) We have meanwhile found that also polymeric [$(Me_3Sn)_3Ir(CN)_6$] reacts readily with ($n$$Pr_4$N)Br to afford excellent single crystals of [($n$$Pr_4$N)$(Me_3Sn)_2Ir(CN)_6 \cdot 2H_2O$], **3d** ($E$ = Sn, M = Ir). The supramolecular architecture of **3d** is essentially the same as that of **3a**, however, the crystal of **3d** was *not disordered* (space group: $P2_12_12_1$; $R1$ for $I > 2\sigma(I)$: 0.0287). The asymmetric unit of **3d** agrees with that found for **3a** by solid-state NMR, and it now appears more likely that in the case of **3a** the "evidence of a disordered structure" might be reinterpreted as evidence of a less symmetric space group than $P2_12_12$.

(c) We have also found that the tetra-*n*-propyl*phosphonium* cation, $(nPr_4P)^+$, is capable to react, like $(nPr_4N)^+$ (vide supra), with [$(Me_3Sn)_3Co(CN)_6$]. According to elemental analysis, solution ^{1}H NMR (D_2O/NaOD) and a single-crystal X-ray study, the new product [$(nPr_4P)(Me_3Sn)_2Co(CN)_6 \cdot 2H_2O$] strongly resembles the product **3a***.

REFERENCES

1. (a) B. M. Lok, T. R. Cannan, and C. A. Messina, *Zeolites* **3,** 282 (1993); (b) "Introduction to Zeolite Science and Practice" (H. Van Bekkum, E. M. Flanigen, and J. C. Jansen, Eds.), Elsevier, Amsterdam, 1991; (c) "Molecular Sieves—Science and Technology" (H. G. Karge and J. Weitkamp, Eds.), Vol. 1–2, Springer, Berlin, 1999; (d) "Catalysis and zeolites" (J. Weitkamp and L. Puppe, Eds.), Springer, Berlin, 1999.
2. (a) R. Robson, B. F. Abrahams, S. R. Batten, R. W. Gable, B. F. Hoskins, and J. Liu, *in* "Supramolecular Architecture" (T. Bein, Ed.), ACS Symposium Ser. 499, Chap. 19, Washington, DC, 1992; (b) C. L. Bowes and G. A. Ozin, *Adv. Mater.* **8,** 13 (1996); (c) T. Iwamoto in "Comprehensive Supramolecular Chemistry" (J. L. Atwood, J. E. D. Davies, D. D. MacNicol, F. Vögtle, and J.-M. Lehn, Eds.), Vol. 6, Pergamon, Oxford, 1996; (d) K. K. Dunbar and R. A. Heintz, *Progr. Inorg. Chem.* **45,** 283 (1997).
3. (a) R. W. Gable, B. F. Hoskins, and R. Robson, *J. Chem. Soc. Chem. Commun.* 762 (1990); (b) B. F. Hoskins and R. Robson, *J. Am. Chem. Soc.* **112,** 1546 (1990).
4. S. Eller, doctoral dissertation, Univ. Hamburg, Germany, 1992.
5. A. K. Brimah, E. Siebel, R. D. Fischer, N. A. Davies, D. C. Apperley, and R. K. Harris, *Organomet. Chem.* **475,** 85 (1994).
6. T. Kitazawa, S. Nishikiori, R. Kuroda, and T. Iwamoto, *J. Chem. Soc. Dalton Trans.* 1029 (1994).
7. P. Schwarz, S. Eller, E. Siebel, T. M. Soliman, R. D. Fischer, D. C. Apperley, N. A. Davies, and R. K. Harris, *Angew. Chem.* **108,** 1611 (1996); *Angew. Chem. Int. Ed. Engl.* **35,** 1525 (1996).
8. (a) E. Siebel, R. D. Fischer, J. Kopf, N. A. Davies, D. C. Apperley and R. K. Harris, *Inorg. Chem. Commun.* 1, 346 (1998); (b) E.-M. Poll and R. D. Fischer, *Inorg. Chem. Commun.*, in press.
9. P. Schwarz, E. Siebel, R. D. Fischer, N. A. Davies, D. C. Apperley, and R. K. Harris, *Chem. Eur. J.* **4,** 919 (1998).
10. A. M. A. Ibrahim, *J. Organomet. Chem.* **556,** 1 (1998).
11. F. X. Ryan, US patent 4851 200 (1989).
12. (a) K. Yünlü, N. Höck, and R. D. Fischer, *Angew. Chem.* **97,** 863 (1985); *Angew. Chem. Int. Ed. Engl.* **24,** 879 (1985); (b) U. Behrens, A. K. Brimah, T. M. Soliman,D. Fischer, D. C. Apperley, N. A. Davies, and R. K. Harris, *Organometallics* **11,** 1718 (1992).
13. See "The Rietveld Method" (R. A. Young, Ed.), p. 98, Oxford Univ. Press, Oxford, 1993.
14. D. C. Apperley, N. A. Davies, R. K. Harris, A. K. Brimah, S. Eller and R. D. Fischer, *Organometallics* **9,** 2672 (1990).
15. (a) S. Eller, P. Schwarz, A. K. Brimah, R. D. Fischer, D. C. Apperley, N. A. Davies, and R. K. Harris, *Organometallics* **12,** 3232 (1993); (b) R. E. Dinnebier, E. Siebel, and R. D. Fischer, unpublished results of a Rietveld analysis of the XRD of **1**.
16. S. Eller, P. Brandt, A. K. Brimah, P. Schwarz, and R. D. Fischer, *Angew. Chem.* **101,** 1274 (1989); *Angew. Chem. Int. Ed. Engl.* **28,** 1263 (1989).
17. D. S. Reddy, B. S. Goud, K. Paneerselvam, and G. R. Desiraju, *J. Chem. Soc. Chem. Commun.* 663 (1993).
18. R. K. Harris, M. Sünnetçioglu, and R. D. Fischer, *Spectrochim. Acta* **50**A, 2069, (1994).
19. R. K. Harris and A. C. Olivieri, *Prog. NMR Spectrosc.* **25,** 435 (1992).
20. J. Skibsted, N. C. Nielsen, H. Bildsoe, and H. J. Jakobsen, *J. Am. Chem. Soc.* **115,** 7351 (1993)
21. (a) J. M. Harrowfield, M. I. Ogden, W. R. Richmond, B. W. Skelton, and A. H. White, *J. Chem. Soc. Perkin Trans.* **2,** 2183 (1993); (b) P. S. Bates, R. Kataky, and D. Parker, *Analyst* **119,** 181 (1994); (c) S. Tomàs, R. Prohens, M. Vega, M. C. Rotger, P. M. Deyà, P. Ballester, and A. Costa, *J. Org. Chem.* **61,** 9394 (1996); (d) M. Scherer, D. L. Caulder, D. W. Johnson, and K. N. Raymond, *Angew. Chem.* **11,** 1690 (1999); *Angew. Chem. Int. Ed. Engl.* **38,** 1588 (1999).
22. (a) G. T. Kokotailo, S. L. Lawton, and D. H. Olson, *Nature* **272,** 437 (1978); (b) L. Xiaoyang, S. Wenhui, W. Yifeng, and Z. Xudong, *J. Chem. Soc. Chem. Commun.* 902 (1992).
23. B. Burger, K. Haas-Santo, M. Hunger, and J. Weitkamp, *Chem. Ing. Tech.* **71,** 732 (1999)
24. (a) Hosts of urea/allophanate$^-$: T. C. W. Mak, W. H. Yip, and Q. Li, *J. Am. Chem. Soc.***117,** 11995 (1995); hosts of urea/dihydrogen borate$^-$: Q. Li, F. Xue, and T. C. W. Mak, *Inorg. Chem.* **38,** 4142 (1999).